

Functional renormalization group study of Nambu–Jona-Lasinio model at finite temperature and density in external magnetic field

Ken-Ichi Aoki,^{1,*} Hidenari Uoi^{†,1,‡} and Masatoshi Yamada^{1,§}

¹*Institute for Theoretical Physics, Kanazawa University, Kanazawa 920-1192, Japan*

We study the Nambu–Jona-Lasinio (NJL) model at finite temperature and finite density in an external magnetic field using the Functional Renormalization Group (FRG). The dependence of the position of UltraViolet Fixed Point (UVFP) of the four-fermi coupling constant on temperature, density and external magnetic field is investigated and we obtain the chiral phase structure. The UVFP at low temperature and finite chemical potential oscillates in small external magnetic field, which can be interpreted as the de-Haas–van-Alfen effect. We also find that the external magnetic field moves the chiral phase boundary towards the symmetric side at low temperature and high density region.

I. INTRODUCTION

The phase diagram and the equation of state of QCD have been studied as important subjects in the elementary particle physics. Particularly QCD matter in an external magnetic field has drawn much attention by several reasons. It is known that the neutron stars, which are high baryonic density stars, generate strong external magnetic fields ($B \sim 10^{14}$ Gauss) [1]. In heavy-ion collision experiments quite strong external magnetic fields ($B \sim 10^{19}$ Gauss) are predicted to exist [2–6]. Furthermore, it is indicated that extremely strong magnetic fields ($B \sim 10^{23}$ Gauss) are generated via the cosmological electroweak phase transition [7] and quark-hadron phase transition [8]. Thus, QCD matter in strong magnetic fields with $|eB| \sim \Lambda_{\text{QCD}}^2$ has been common in our universe.

It is known within the analysis of chiral effective models that under the external magnetic field the chiral symmetry is always broken due to the dimensional reduction. This phenomenon is called the magnetic catalysis [9–15], and the chiral restoration temperature increases with stronger magnetic field. On the other hand, for a fixed low temperature the chiral restoration density decreases [16–18].

The recent lattice simulation [19] for QCD with an external magnetic field indicates that the critical restoration temperature decreases with stronger magnetic field, which is called the inverse magnetic catalysis or the magnetic inhibition [20–24]. Although this phenomenon has been studied by various approaches, nothing has been agreed widely.

In this paper we analyze the NJL model describing the Dynamical Chiral Symmetry Breaking (D χ SB) [25–27] in a strong magnetic field at finite temperature and finite density by using the Functional Renormalization

Group (FRG) [28–32]. The basic properties of this system such as the Renormalization Group (RG) flow equations and the fixed point structure were studied in many papers [18, 33–37]. This work investigates the behavior of the RG flow of the four-fermi coupling constant and analyze in detail the phase diagram in the NJL model with an external magnetic field.

This paper is organized as follows: the formulation is given in the next section. Our results for structures of fixed points, the phase diagram and the large- N non-leading effects are presented in section III. We summarize and discuss the results in section IV.

II. THE NJL MODEL AND ITS RG EQUATIONS

In this section the RG flow equation of the four fermi coupling constant and its structure in an external magnetic field at finite temperature and density are briefly introduced. The energy dispersion relation of a massless quark with electric charge q in external magnetic field $\mathbf{B} = (0, 0, B)$ is $E_n^2 = (2n + 1 + s)|qB| + p_z^2$ where $s = \pm 1$ is the Zeeman splitting by interaction between the spin of quark and B . The quantum number $n = 0, 1, 2, \dots$ is the Landau level, and especially the case of $n = 0$ and $s = -1$ is called the Lowest Landau level (LLL). In case of LLL the dynamics of the quarks is effectively described as an $1 + 1$ dimensional system.

We adopt the following truncated effective action with $U_L(1) \times U_R(1)$ chiral symmetry in the Euclidean space,

$$\Gamma_\Lambda = \int_0^\beta d\tau \int d^3x [\bar{\psi}(\not{\partial} + \mu + q\not{A})\psi - \frac{G_\Lambda}{2} \{(\bar{\psi}\psi)^2 + (\bar{\psi}i\gamma_5\psi)^2\}], \quad (1)$$

where the external vector potential A_μ is defined to give $\mathbf{B} = (0, 0, B) = \text{rot } \mathbf{A}$. The external field A_μ has several representations due to the gauge degrees of freedom, e.g., the symmetric gauge: $A_\mu = (0, By/2, -Bx/2, 0)$ or the Landau gauge: $A_\mu = (0, 0, Bx, 0)$.

The effective action is governed by the Wetterich equa-

[†]H. U. belonged to the Institute until March 2014.

*Electronic address: aoki@hep.s.kanazawa-u.ac.jp

[‡]Electronic address: huoi@hep.s.kanazawa-u.ac.jp

[§]Electronic address: masay@hep.s.kanazawa-u.ac.jp

tion [38]. In our case it reads

$$\partial_t \Gamma_\Lambda[\psi, \bar{\psi}] = -\text{Tr} \left[\frac{\partial_t R_\Lambda}{\Gamma_\Lambda^{(1,1)} + R_\Lambda} \right], \quad (2)$$

where $\Gamma_\Lambda^{(i,j)}$ denotes the i -th (j -th) left (right)-hand side derivative of the effective action Γ_Λ with respect to ψ ($\bar{\psi}$). The cut-off profile function R_Λ controls the shell momentum integration, realizing the coarse-graining. Here, we employ the 3d optimized cut-off function [39, 40],

$$R_\Lambda(\mathbf{p}) = i\mathbf{p} \left(\frac{\Lambda}{|\mathbf{p}|} - 1 \right) \theta(1 - |\mathbf{p}|/\Lambda). \quad (3)$$

The momentum mode integral at finite temperature in the external magnetic field takes the following form,

$$2 \int \frac{d^4 p}{(2\pi)^4} \rightarrow T \sum_{m=-\infty}^{\infty} \frac{|qB|}{2\pi} \sum_{l=0}^{\infty} \alpha_l \int \frac{dp_z}{2\pi}, \quad (4)$$

where m is the Matsubara mode number, the factor 2 in the LHS and $\alpha_l = 2 - \delta_{l,0}$ in the RHS are the spin-degeneracy factors. We also rewrite the Landau level as $2n + 1 + s \equiv 2l$ with $l = 0, 1, 2, \dots$.

The details of the derivation of RG flow equations in this system are given in the literature [18]. The RG equations for the effective action (1) are reduced as follows:

$$\partial_t g = -2g + g^2 \left(4N_c J_0(\tilde{T}, \tilde{\mu}, \tilde{B}) - J_1(\tilde{T}, \tilde{\mu}, \tilde{B}) \right), \quad (5)$$

$$\partial_t \tilde{T} = \tilde{T}, \quad (6)$$

$$\partial_t \tilde{\mu} = \tilde{\mu}, \quad (7)$$

$$\partial_t \tilde{B} = 2\tilde{B}, \quad (8)$$

where g is the dimensionless rescaled four-fermi coupling constant $G_\Lambda \Lambda^2 / 2\pi^2$, and \tilde{T} , $\tilde{\mu}$ and \tilde{B} are dimensionless external parameters and ∂_t denotes the derivative with respect to the dimensionless cut-off scale $t = \log(\Lambda_0/\Lambda)$. The threshold functions J_0 and J_1 are defined by

$$J_0(\tilde{T}, \tilde{\mu}, \tilde{B}) = \frac{|q\tilde{B}|}{4} \sum_{l=0}^{\lfloor \frac{1}{2|q\tilde{B}} \rfloor} \alpha_l \sqrt{1 - 2l|q\tilde{B}|} \times \{1 - n_+ - n_- - \partial_t(n_+ + n_-)\}, \quad (9)$$

$$J_1(\tilde{T}, \tilde{\mu}, \tilde{B}) = \frac{|q\tilde{B}|}{4} \sum_{l=0}^{\lfloor \frac{1}{2|q\tilde{B}} \rfloor} \alpha_l \sqrt{1 - 2l|q\tilde{B}|} \times \left\{ \frac{1}{(1 + \tilde{\mu})^2} \left(\frac{1}{2} - n_+ \right) + \frac{1}{(1 - \tilde{\mu})^2} \left(\frac{1}{2} - n_- \right) - \frac{1}{1 + \tilde{\mu}} \partial_t n_+ - \frac{1}{1 - \tilde{\mu}} \partial_t n_- \right\}. \quad (10)$$

The Gauss symbol $[x]$ denotes the greatest integer that is less or equal to x . The Fermi-Dirac distribution functions n_\pm are defined as

$$n_\pm = \frac{1}{e^{\beta(\Lambda \pm \mu)} + 1} = \frac{1}{e^{\tilde{\beta}(1 \pm \tilde{\mu})} + 1}. \quad (11)$$

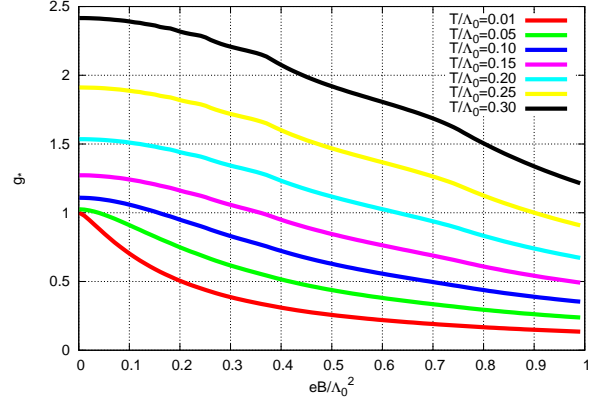


FIG. 1: The dependence of the position of UVFP g^* on the external magnetic field at finite temperature with the vanishing density in the large- N leading approximation.

The factor 4 and N_c in RHS of Eq. (5) are the numbers of degrees of freedom of spinor and color of fermionic fields, respectively. The large- N leading approximation neglects the quantum corrections corresponding to the J_1 term in Eq. (5).

III. RESULTS

A. Fixed Point

In this subsection we analyze the structure of the UltraViolet Fixed Point (UVFP) g^* which satisfies $\beta(g^*) = 0$ for the β function of g in Eq. (5). The four-fermi coupling constant g corresponds to the chiral susceptibility $\langle (\bar{\psi}\psi)^2 \rangle$. Therefore, the RG flow equation of g with the initial value $g_0 > g^*$ diverges at a critical scale where the D χ SB with the second order phase transition turns on.

In case of strong B in which the LLL approximation is effective with vanishing T and μ , the beta function of g is given by

$$\beta_g = -2g + N_c g^2 |q\tilde{B}|. \quad (12)$$

It implies that the UVFP and the Gaussian FP ($g^* = 0$) will become degenerated at large t . This property is due to the dimensional reduction [18]. Actually the RG flow of g always diverges for $g_0 > 0$. The thermal and dense effects resolve the degeneracy of the FPs. We investigate the dependence of the position of UVFP on temperature, chemical potential and external magnetic field. The RG equation of the four-fermi coupling constant in the large- N leading approximation is given by

$$\partial_t g = -2g + 4N_c g^2 J_0(\tilde{T}, \tilde{\mu}, \tilde{B}). \quad (13)$$

Here we set the following values: $N_c = 3$ and $q = (2/3)e$. The UVFP g^* of this equation is given by

$$g^* = \frac{1}{6J_0(\tilde{T}, \tilde{\mu}, \tilde{B})}. \quad (14)$$

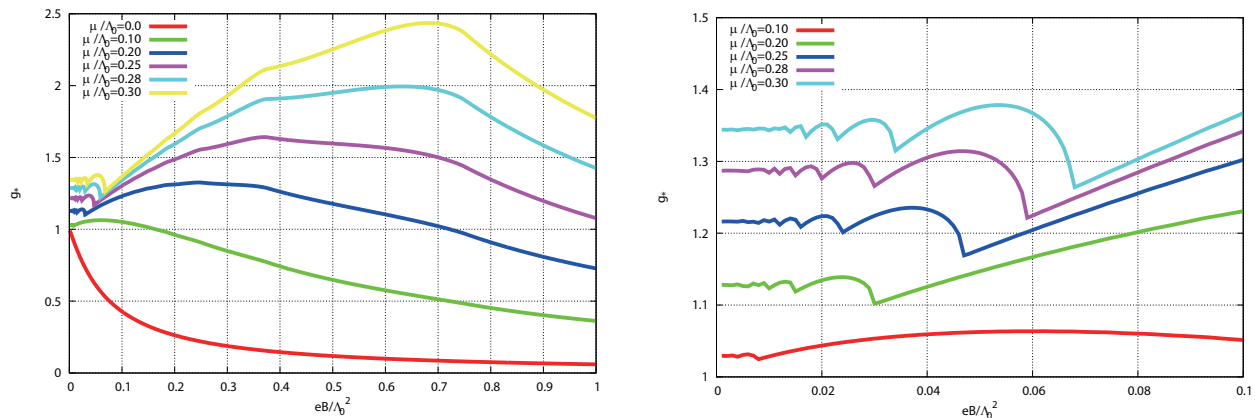


FIG. 2: The dependence of the position of UVFP g^* on the external magnetic field and finite density with fixed temperature ($T/\Lambda_0 = 0.0001$) in the large- N leading approximation. The right-hand side diagram shows the zoom up of the small B region.

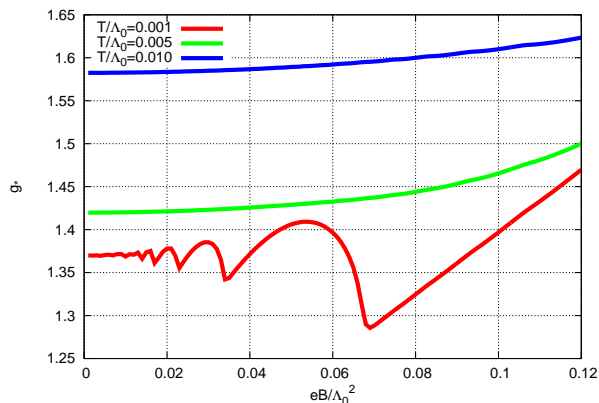


FIG. 3: The dependence of the position of UVFP g^* of Eq. (13) on the external magnetic field with fixed chemical potential ($\mu/\Lambda_0 = 0.10$) and several temperatures in the large- N leading approximation.

The position of UVFP in finite temperature, finite external magnetic field and vanishing chemical potential is shown in Fig. 1. We find that g^* decreases monotonically with increasing B for any temperature, thus, the magnetic catalysis occurs. This result corresponds to earlier studies of the chiral effective models (see Ref. [14] for example).

The change of the position of the UVFP caused by finite density and finite external magnetic field with a fixed low temperature ($T/\Lambda_0 = 0.0001$) is shown in Fig. 2. For smaller B region the UVFP shown in the right-hand side panel of Fig. 2 oscillates. This behavior can be interpreted as the de-Haas–van-Alfen (dHvA) effect which is observed in some related studies, e.g., in the color superconducting matter [41], in the holographic matter [16, 17] and in the NJL model with the mean field approximation [42]. That is, the oscillatory behavior comes from the processes that each Landau level $2|qB|n$ crosses the fermi surface μ^2 . The end point of oscillation corresponds to

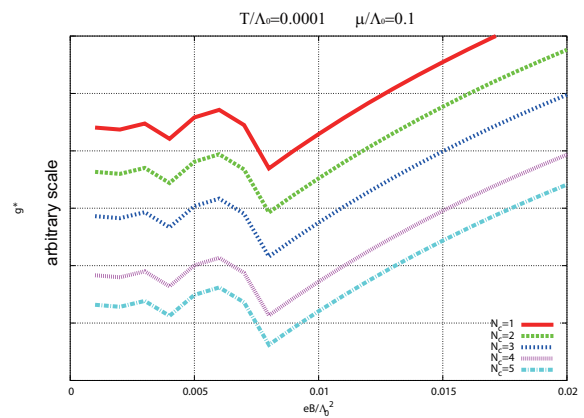


FIG. 4: The dependence of the position of UVFP g^* for various number of color N_c . The scale of the vertical axis is arbitrary

the case that the first Landau level ($n = 1$) just overlaps with the fermi surface. Therefore beyond the oscillatory region only the LLL can contribute. For example, in case of $\mu/\Lambda_0 = 0.2$ the oscillation ceases at $eB/\Lambda_0^2 \simeq 0.03$. These values satisfy the relation $2|qB| = 2|\frac{2}{3}eB| \simeq \mu^2$. The dHvA effect disappears at higher temperature (see Fig. 3). The Landau level and the fermi surface don't depend on the number of flavor and color, hence, this phenomenon is not affected by them as shown in Fig. 4.

After the oscillation ceases, the UVFP g^* increases with increasing B , which means that the inverse magnetic catalysis occurs. Moreover, we point out that the UVFP decreases for larger B . It seems that the effect of finite density decouples for larger external magnetic field because the magnetic field at the peak is proportional to the chemical potential. So far, there are no clear explanation of this behavior.

We investigate the impact of the large- N non-leading corrections, using Eq. (5) with J_1 term included. The comparison of the position of UVFP g^* between the

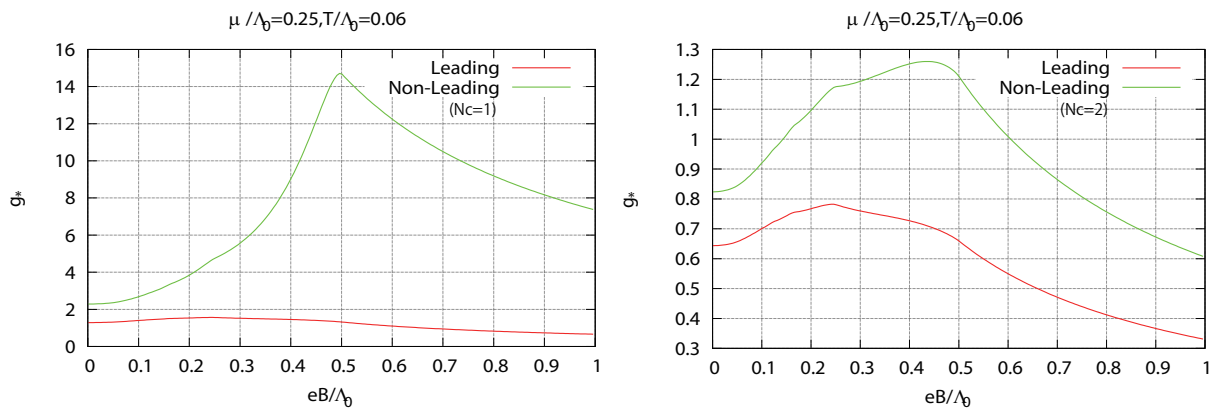


FIG. 5: Comparison of the position of UVFP g^* between the large- N leading case and non-leading case with $N_c = 1$ (left) and $N_c = 2$ (right).

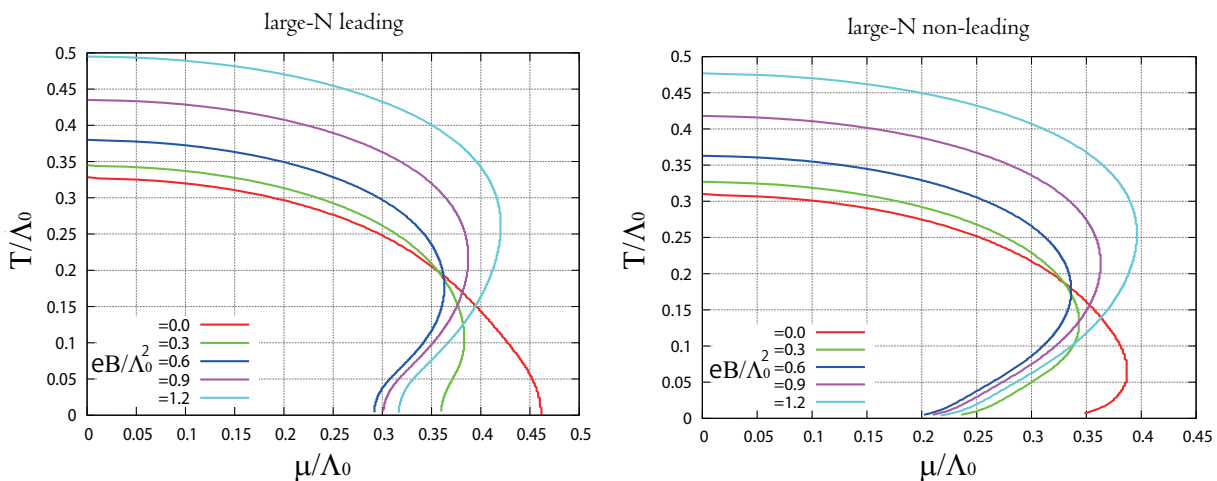


FIG. 6: The chiral phase diagram on $\tilde{\mu}$ - \tilde{T} plane. The left and right figures are the large- N leading case and non-leading case, respectively.

large- N leading case and non-leading case with $N_c = 1$ and $N_c = 2$ is shown in Fig. 5. The large- N non-leading corrections make the UVFP g^* larger in the whole region of B . However, the qualitative magnetic behavior of the UVFP does not change much by inclusion of the large- N non-leading effects.

B. Phase diagram

We show the phase diagrams on $\tilde{\mu} - \tilde{T}$ plane with fixed external magnetic field in Fig. 6. We evaluate the RG equation of the inverse four-fermi coupling constant in order to obtain the four-fermi coupling constant at the infrared limit [37]. Note that the phase boundaries in these phase diagrams does not necessarily mean the true chiral phase transition point. These boundaries represent the instability of the chiral symmetric vacuum, which is the phase transition point only for the second order transition. For the first order phase transition, the true transi-

sition point is somewhat moved to the symmetric side. Here we set the dimensionless rescaled inverse four-fermi coupling constant $1/g = 0.182$ at the initial scale $t = 0$, whose RG flow at vanishing temperature and density goes to the broken phase at the infrared scale.

First, we discuss the large- N leading case. At high temperature region, the phase boundaries move higher temperature side with increasing B , that is, the magnetic catalysis occurs. On the other hand, the inverse magnetic catalysis appears at low temperature region. There, the phase boundaries move towards the lower density side with increasing B . Then for large B , they turns back towards the higher density side. This behavior is observed also in the mean-field approximation [42].

Next, we discuss the large- N non-leading effects. At low temperature, the phase boundary even with the vanishing B turns over towards the lower density side. This occurs due to the singularity at the fermi surface (see [37]).

IV. SUMMARY AND DISCUSSION

In this paper, we have investigated the dependence of the UVFP of the four-fermi coupling constant in the NJL model at finite temperature and density under the external magnetic field by using the functional renormalization group. The UVFP decreases monotonically with increasing magnetic field at finite temperature and vanishing chemical potential, thus, the magnetic catalysis occurs. At finite chemical potential and a fixed low temperature the UVFP oscillates depending on the external magnetic field due to the de-Haas-van-Alfen effect. This effect vanishes at higher temperature. The UVFP increase with increasing magnetic field after the oscillatory region, which means the inverse magnetic catalysis occurs. However, even larger external magnetic field turns the inverse magnetic catalysis into the magnetic catalysis.

The chiral phase diagram has been investigated. The magnetic catalysis is observed at high temperature and low density. On the other hand, at low temperature and high density the inverse magnetic catalysis occurs with large external magnetic field.

The large- N non-leading effects do not drastically change the qualitative behaviors in our system.

In order to investigate the cut-off scheme dependence we analyzed the system with the $1d$ optimized cut-off function [43],

$$R_\Lambda(p_z) = ip_z \gamma_z \left(\frac{\Lambda}{|p_z|} - 1 \right) \theta(1 - |p_z|/\Lambda). \quad (15)$$

The threshold functions are shown in Appendix A. As a result, the qualitative behaviors such as the dependence of UVFP on the thermal effects and the phase diagram do not change. Hence it seems that the behavior of the UVFP and the phase diagram reported in this paper are quite stable against the cut-off profile.

We hope these analyses should motivate more elab-

orate studies in future by using the re-bosonization method [44–48] or the weak solution method [49]. More precise analyses should be done.

Acknowledgements

We thank Motoi Tachibana and Daisuke Sato for fruitful discussions and comments, and Hokuriku–Shin-etsu Winter school supported by Yukawa Institute for Theoretical Physics (YITP-S-13-06). M. Y. is supported by a Grant-in-Aid for JSPS Fellows (No. 25-5332). K-I. A. is supported by JSPS Grant-in-Aid for Challenging Exploratory Research (No. 25610103).

Appendix A: The threshold function with $1d$ optimized cut-off function

Here, we give the threshold functions by using the $1d$ optimized cut-off function (15) in the RG equation of four-fermi coupling constant. We have

$$I_0(\tilde{T}, \tilde{\mu}, \tilde{B}) = \frac{|q\tilde{B}|}{4} \left[-1 + \frac{\zeta\left(\frac{3}{2}, \frac{1}{2|e\tilde{B}|}\right)}{\sqrt{2}|e\tilde{B}|^{3/2}} - \sum_{l=0}^{\infty} \alpha_l \left\{ \frac{(n_+ + n_-)}{\tilde{\epsilon}_l^3} - \frac{\partial_t(n_+ + n_-)}{\tilde{\epsilon}_l} \right\} \right], \quad (A1)$$

$$I_1(\tilde{T}, \tilde{\mu}, \tilde{B}) = \frac{|q\tilde{B}|}{4} \sum_{l=0}^{\infty} \alpha_l \left[\frac{1}{\tilde{\epsilon}_l(\tilde{\epsilon}_l^+)^2} \left(\frac{1}{2} - n_+ \right) + \frac{1}{\tilde{\epsilon}_l(\tilde{\epsilon}_l^-)^2} \left(\frac{1}{2} - n_- \right) - \frac{\partial_t n_+}{\tilde{\epsilon}_l^+} - \frac{\partial_t n_-}{\tilde{\epsilon}_l^-} \right], \quad (A2)$$

where $\zeta(s, x)$ is the Hurwitz zeta function, n_\pm are given in Eq. (11) and $\tilde{\epsilon}_l^\pm = \tilde{\epsilon}_l \pm \tilde{\mu}$ with $\tilde{\epsilon}_l^2 = 1 + 2l|q\tilde{B}|$. The RG equation of the four-fermi coupling constant is obtained by replacing J_0 and J_1 with I_0 and I_1 , respectively.

-
- [1] R. C. Duncan and C. Thompson, *Astrophys.J.* **392**, L9 (1992).
 - [2] D. E. Kharzeev, L. D. McLerran, and H. J. Warringa, *Nucl.Phys.* **A803**, 227 (2008), 0711.0950.
 - [3] K. Fukushima, *J.Phys.* **G39**, 013101 (2012), 1108.2939.
 - [4] K. Fukushima, D. E. Kharzeev, and H. J. Warringa, *Phys.Rev.* **D78**, 074033 (2008), 0808.3382.
 - [5] K. Fukushima, *Prog.Theor.Phys.Suppl.* **193**, 15 (2012).
 - [6] K. Fukushima, *Lect.Notes Phys.* **871**, 241 (2013), 1209.5064.
 - [7] T. Vachaspati, *Phys.Lett.* **B265**, 258 (1991).
 - [8] B.-l. Cheng and A. V. Olinto, *Phys.Rev.* **D50**, 2421 (1994).
 - [9] K. Klimenko, *Theor.Math.Phys.* **89**, 1161 (1992).
 - [10] K. Klimenko, *Z.Phys.* **C54**, 323 (1992).
 - [11] V. Gusynin, V. Miransky, and I. Shovkovy, *Phys.Rev.Lett.* **73**, 3499 (1994), hep-ph/9405262.
 - [12] V. Gusynin, V. Miransky, and I. Shovkovy, *Phys.Rev.* **D52**, 4718 (1995), hep-th/9407168.
 - [13] V. Gusynin, V. Miransky, and I. Shovkovy, *Phys.Lett.* **B349**, 477 (1995), hep-ph/9412257.
 - [14] V. Gusynin, V. Miransky, and I. Shovkovy, *Nucl.Phys.* **B462**, 249 (1996), hep-ph/9509320.
 - [15] I. Shushpanov and A. V. Smilga, *Phys.Lett.* **B402**, 351 (1997), hep-ph/9703201.
 - [16] F. Preis, A. Rebhan, and A. Schmitt, *JHEP* **1103**, 033 (2011), 1012.4785.
 - [17] F. Preis, A. Rebhan, and A. Schmitt, *Lect.Notes Phys.* **871**, 51 (2013), 1208.0536.
 - [18] K. Fukushima and J. M. Pawłowski, *Phys.Rev.* **D86**, 076013 (2012), 1203.4330.
 - [19] G. Bali, F. Bruckmann, G. Endrodi, Z. Fodor, S. Katz, et al., *JHEP* **1202**, 044 (2012), 1111.4956.
 - [20] K. Fukushima and Y. Hidaka, *Phys.Rev.Lett.* **110**,

- 031601 (2013), 1209.1319.
- [21] T. Kojo and N. Su, Phys.Lett. **B720**, 192 (2013), 1211.7318.
- [22] F. Bruckmann, G. Endrodi, and T. G. Kovacs, JHEP **1304**, 112 (2013), 1303.3972.
- [23] J. Chao, P. Chu, and M. Huang, Phys.Rev. **D88**, 054009 (2013), 1305.1100.
- [24] E. Fraga, B. Mintz, and J. Schaffner-Bielich, Phys.Lett. **B731**, 154 (2014), 1311.3964.
- [25] Y. Nambu and G. Jona-Lasinio, Phys.Rev. **122**, 345 (1961).
- [26] Y. Nambu and G. Jona-Lasinio, Phys.Rev. **124**, 246 (1961).
- [27] T. Hatsuda and T. Kunihiro, Phys.Rept. **247**, 221 (1994), hep-ph/9401310.
- [28] K. Aoki, Int.J.Mod.Phys. **B14**, 1249 (2000).
- [29] J. Berges, N. Tetradis, and C. Wetterich, Phys.Rept. **363**, 223 (2002), hep-ph/0005122.
- [30] J. M. Pawłowski, Annals Phys. **322**, 2831 (2007), hep-th/0512261.
- [31] H. Gies, Lect.Notes Phys. **852**, 287 (2012), hep-ph/0611146.
- [32] J. Braun, J.Phys. **G39**, 033001 (2012), 1108.4449.
- [33] K.-I. Aoki, K. Morikawa, J.-I. Sumi, H. Terao, and M. Tomoyose, Prog.Theor.Phys. **102**, 1151 (1999), hep-th/9908042.
- [34] J. Braun, W. A. Mian, and S. Rechenberger (2014), 1412.6025.
- [35] M. Mitter, J. M. Pawłowski, and N. Strodthoff, Phys.Rev. **D91**, 054035 (2015), 1411.7978.
- [36] N. Mueller and J. M. Pawłowski (2015), 1502.08011.
- [37] K.-I. Aoki and M. Yamada (2015), 1504.00749.
- [38] C. Wetterich, Phys.Lett. **B301**, 90 (1993).
- [39] D. F. Litim, Phys.Rev. **D64**, 105007 (2001), hep-th/0103195.
- [40] D. F. Litim and J. M. Pawłowski, JHEP **0611**, 026 (2006), hep-th/0609122.
- [41] K. Fukushima and H. J. Warringa, Phys.Rev.Lett. **100**, 032007 (2008), 0707.3785.
- [42] T. Inagaki, D. Kimura, and T. Murata, Prog.Theor.Phys. **111**, 371 (2004), hep-ph/0312005.
- [43] K. Kamikado and T. Kanazawa, JHEP **1403**, 009 (2014), 1312.3124.
- [44] K.-I. Aoki, K. Morikawa, J.-I. Sumi, H. Terao, and M. Tomoyose, Phys.Rev. **D61**, 045008 (2000), hep-th/9908043.
- [45] H. Gies and C. Wetterich, Phys.Rev. **D65**, 065001 (2002), hep-th/0107221.
- [46] H. Gies and C. Wetterich, Phys.Rev. **D69**, 025001 (2004), hep-th/0209183.
- [47] S. Floerchinger and C. Wetterich, Phys.Lett. **B680**, 371 (2009), 0905.0915.
- [48] J. Braun, L. Fister, J. M. Pawłowski, and F. Rennecke (2014), 1412.1045.
- [49] K.-I. Aoki, S.-I. Kumamoto, and D. Sato, PTEP **2014**, 043B05 (2014), 1403.0174.